ELSEVIER

PII: S0266-3538(98)00038-4

Composites Science and Technology **58** (1998) 1727–1739

Printed in Great Britain
0266-3538/98 $19.00—see front matter

A COMPARISON OF CALCULATED AND MEASURED DEBOND LENGTHS FROM FIBER PUSH-OUT TESTS

V. T. Bechel[a]* & N. R. Sottos[b]

[a]*Nonmetallic Structural Materials Branch, AFRL/MLBC, Building 654, 2941 P Street Suite 1, Wright-Patterson AFB, OH 45433-7750, USA*

[b]*Theoretical and Applied Mechanics Department, University of Illinois at Urbana-Champaign, Champaign, IL, USA*

(Received 10 August 1997; revised 2 October 1997; accepted 6 February 1998)

Abstract

A procedure involving iterative finite-element analyses has been developed for the accurate prediction of the debond length as a function of force by using the progressive debonding load/deflection data from fiber push-out tests conducted on a polyester/epoxy model composite with a thickness of approximately 2·5 fiber diameters. The finite-element simulation included loads due to chemical shrinkage of the matrix during cure as well as the boundary conditions corresponding to the exact probe and sample support dimensions. The resulting debond lengths corresponded to within 7% of the measured debond lengths. Fracture energy was also determined by the finite-element method by computing the change in potential energy when incrementing the interface crack length by 0·1% of the total crack length and subtracting the increase in the energy dissipated by friction. © *1998 Elsevier Science Ltd. All rights reserved*

Keywords: A. polymer-matrix composites, B. debonding, B. fracture, B. friction, C. finite-element analysis

1 INTRODUCTION

The fiber push-out test has become a popular method of determining the interfacial shear strength and the friction law for the interface in fiber-reinforced composites. The test involves pushing a single fiber out of a thin slice of composite while measuring applied force and push-out tool displacement. The force/displacement curve recorded during the test is later related to the interface mode-II critical energy release rate and the coefficient of friction between the fiber and matrix by fitting the data to either an analytical or a finite-element solution.

1.1 Shear-lag theory

Approximate theories based on the shear-lag assumption of load transfer by shear from an infinite matrix to an infinitely long fiber have been developed to convert the force/displacement data from push-out experiments to interface properties.[1–5] The requirements of shear-lag theory can be difficult to meet. Since tests on thick samples in which the debond can grow far away from the surface are often not possible without damage to the punch and/or fiber, fiber push-out tests are sometimes performed on thin samples. In some cases, push-out samples have been fabricated as thin as three fiber diameters to make complete debonding possible.[6,7] The inapplicability of shear-lag solutions to thin samples was verified by Bechel and Sottos,[8] who conducted experiments to measure the debond length in a polyester/epoxy model composite. The experiments indicated that, although easy to apply, the most advanced shear-lag theory for fiber push-out developed by both Liang and Hutchinson[4] and Kerans and Parthasarathy[5] (subsequently referred to as the LH and KP solution in this paper) overestimated the interfacial critical energy release rate in a polyester/epoxy model composite with a sample thickness of 2·5 fiber diameters.

The LH and KP solution is not applicable to relatively thin samples for several reasons. The debond never grows far from the top surface before total debond. Consequently, the length over which surface effects (i.e. non-uniform interfacial residual shear and radial stress) must be considered as a significant portion of the debonded part of the fiber. The actual boundary conditions corresponding to a punch diameter smaller than the fiber diameter and a support hole diameter larger than the fiber diameter are not modeled. The ratio of the punch to fiber diameter influences the displacement due to a given punch load,[9] and the larger support hole diameter may cause the compliance of the remaining bonded portion of the sample (referred to as 'sample compliance' in the push-out literature) to increase as the debond grows. The usual method of deriving the displacement appropriate for shear-lag assumes sample compliance is constant. Finally, the possibility of a portion of the interface separating is not allowed by the LH and KP solution.

*To whom correspondence should be addressed.

The experiments by Bechel and Sottos[8] consisted of observing the development of the photoelastic fringes in the matrix during the progressive debonding phase of fiber push-out tests carried out in a circular polariscope. A concentration of the isochromatic fringes along the interface indicated the location of the debond tip. For polyester/epoxy samples that were thin enough to allow total debonding without damage to the top of the fiber, shear-lag under-predicted the debond length which resulted in an overestimate of the strength of the interface. The focus of the current work is to present a relatively simple procedure for converting push-out data from experiments to a critical energy release rate, G_{IIc}, that will be accurate for a sample of arbitrary thickness. Although this method, which may include several successive finite-element runs, requires more effort than curve fitting one or two shear-lag equations, the time required is not prohibitive.

1.2 Finite-element method

The finite-element method addresses all the concerns noted above. The shear-lag assumption is not necessary, since the complete set of coupled partial differential equations from the formulation of an isotropic linear elastic problem is solved, and boundary conditions that more closely simulate processing and fiber push-out can be implemented. Additionally, the interface elements used in this study allow a loss of contact if a tensile radial stress results during loading.

Kallas *et al.*[10] used the finite-element method to calculate the stress distribution for a fully bonded thin slice fiber push-out sample of sapphire fibers in a niobium matrix under typical pre-debonding loads. Axisymmetric finite elements were used. Kallas and coworkers showed that the difference in magnitude between the peak in the shear stress (an artifact of the mesh's inability to capture the stress singularity) at the top and at the bottom of the interface is affected by the sample thickness and the support hole size relative to the fiber diameter. No interface strength parameter was calculated, since a crack was not included in the model. Ghosn *et al.*[11] did similar work with a three-dimensional finite-element mesh to model the linear groove in the push-out sample support more rigorously. A groove is often employed instead of a circular hole to permit more fibers to be push-out tested in less time.

Kishore *et al.*[12,13] developed a method of finding the stress intensity factor by matching a global finite-element solution to the asymptotic solution at the top of the interface for a fiber pull-out geometry (fully bonded interface). With the appropriate asymptotic stress field, this operation could also be used to calculate the stress intensity factor at the crack tip in a fiber push-out problem if the debond length has already been determined. Since a focused mesh of circular rings of elements in the plane of the cross section and concentric with the crack tip is required, this method may be too time-intensive when checking the critical stress intensity factor at several debond lengths.

Beckert and Lauke[14] used a finite-element analysis to determine the interfacial energy release rate in a fiber pull-out simulation in which an interface crack extended from the top surface to a point along the interface below the surface. This method could be applied to calculating interfacial fracture energy in the push-out test if the sign of the applied load was changed and the embedded fiber was allowed to extend through the entire sample. Friction and residual stresses were not included in the model, and the length of the debond would have to be determined by some other method.

Chandra and Ananth[15] included residual stresses due to processing. Debond length was predicted by finite-element simulations of the fiber push-out test but was not compared with experimentally measured debond length data. A maximum shear stress, $(\tau_{rz})_{max}$, along the interface was chosen and the interface in the model failed when $(\tau_{rz})_{max}$ was exceeded. Force/displacement curves were generated by finite-element analyses for several interface strengths and then compared with an experimental force/displacement curve. The interface strength that corresponded to the best curve fit was chosen. This method is powerful because the location of initial debonding and even the possibility of debond growth occurring from both ends of the sample at the same time could be predicted and included in the model. A drawback of Chandra and Ananth's formulation is their use of a maximum shear stress criterion for characterizing resistance to growth of a sharp crack.

The concentric cylinders variational model developed by Tandon and Pagano[16] was used to study the interaction of an annular matrix crack with an interface crack that was composed of opened, slipping and sticking zones in a composite uniformly strained longitudinally. Discretization was required only in the radial direction with the axial and hoop stresses assumed to vary linearly in the radial direction within each element. The same model was employed by Tandon and Pagano[17] for solving fiber push-out problems similar to the problems solved in this study. The formulation of Tandon and Pagano[17] allows the exact boundary conditions imposed on the top and bottom of the push-out sample during testing to be imposed on the model. The interface can open if a tensile interfacial radial stress develops, and Coulomb friction can be incorporated in the slipping zone of the interface. A comparison was made between some of the results from the current work and results from the model of Tandon and Pagano.[17]

The present finite-element solution includes residual stress effects and determines the debond length as a function of force from experimental load-deflection data, independent of a criterion for interface decohesion. Both a top and a bottom debond can be considered if necessary, and the development of a frictional shear stress on the debonded portion(s) of the interface is included with the interface boundary conditions. To

quantify the interface strength, the critical energy-release rate is computed once the debond lengths that corresponded to the critical loads applied during progressive debonding are determined.

2 FINITE-ELEMENT MODEL

The geometry of the fiber push-out problem is shown in Fig. 1. An axisymmetric model is assumed with r as the radial coordinate originating at the fiber central axis and z as the axial coordinate originating at the bottom of the sample. The radii of the punch, fiber and outer edge of the matrix are r_p, r_f and r_o, respectively. A portion of the fiber, l_d, may be debonded, and the sample thickness in the axial direction is denoted by t.

The commercial finite-element code ABAQUS (Hibbitt, Karlsson, and Sorenson, Inc.) was used for the finite-element modeling described in this paper. The fiber push-out sample was modeled with second-order axisymmetric isoparametric (CAX8) elements and second-order axisymmetric frictional interface (INTER3A) elements. The fiber and matrix materials were assumed to be isotropic and linear elastic. The interface elements could sustain only shear stress, τ_{rz}, with a magnitude less than or equal to $|\mu\sigma_{rr}|$ and compressive or zero radial stress, σ_{rr}. The formulation of the interface elements allowed not only separation, but also sliding of finite amplitude if Coulomb friction was exceeded and arbitrary rotation of the surfaces.[18]

The finite-element mesh designed for the push-out problem is shown in Fig. 2. The fiber/matrix interface and top and bottom faces of the sample were densely meshed, since the stresses may change rapidly in those areas and the shape functions representing the variation of displacement within each element may not be able to approximate closely the actual displacement. The stress concentrations at the punch and support hole edges also required a large concentration of elements. Typical meshes contained 2500 to 3000 elements.

The minimum mesh refinement necessary was determined according to two criteria. For problems that did not involve an energy-release-rate calculation, e.g. problems run to calculate debond length or fully slipping problems, the mesh was considered dense enough when further refinement of any portion of the model caused less than a 0·1% change in the resulting total load on the top of the fiber. For problems in which potential energy and frictional energy dissipated were extracted for use in computing the critical energy-release rate, G_{IIc}, an additional requirement was implemented that any further mesh refinement near the interface crack tip caused less than a 1% change in the value of G_{IIc}.

Although the materials were linear elastic, the solution was non-linear owing to contact being lost across part of the interface as the punch load increased and owing to the energy lost from the non-conservative frictional shear stress generated by the debonded portion of the fiber sliding with respect to the matrix. Within each finite-element run the push-out problem was solved in two steps. The thermal/chemical shrinkage load was applied in step one, and the mechanical

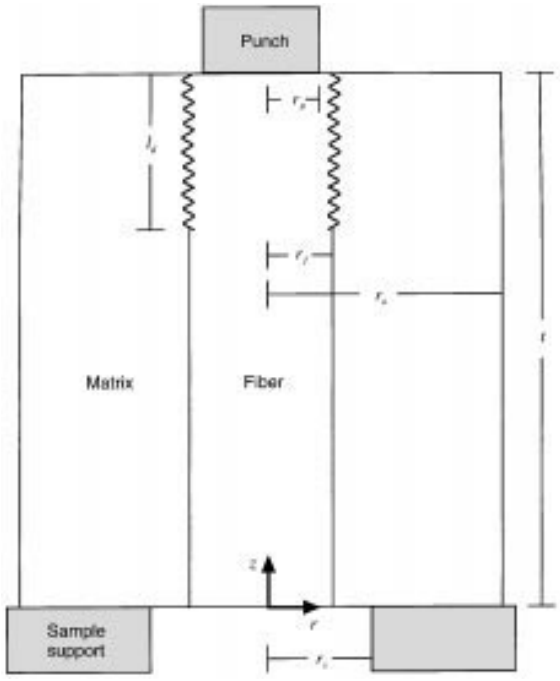

Fig. 1. Schematic of the coordinate axes and relevant dimensions.

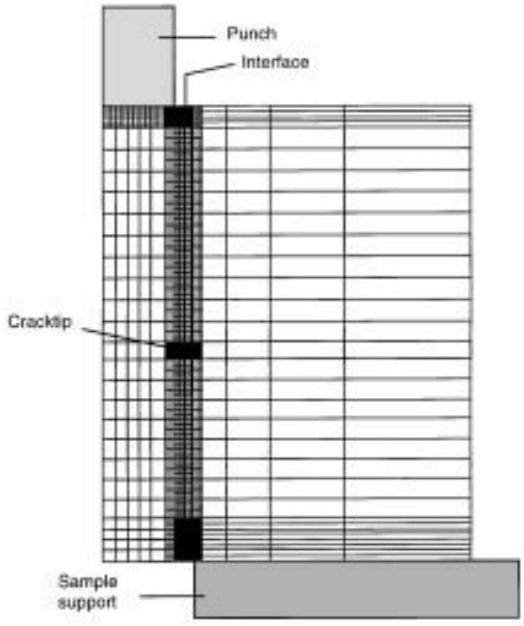

Fig. 2. Finite element mesh constructed to simulate processing and pushout loads.

load was applied to the fiber top face in step two. Within each step, the load was applied in increments. For the first solution attempt, the entire load was applied. If the solution of the field equations was not converging quickly enough according to criteria placed on whether the field equations were satisfied (peak force residual $< 0{\cdot}005$ N) and the largest correction to a nodal variable (largest change in incremental displacement $< 0{\cdot}01\ \mu$m), the load was applied in smaller increments. Within each increment ABAQUS solved the governing balance equations iteratively using a modified Newton's method. If, at the end of an iteration, one or more of the constraints in any of the interface elements was violated, the interface element(s) in question was(were) allowed to open or slip, and a new iteration was started. Typically, from 1 to 16 increments per step and less than 10 iterations per increment were necessary, depending on the debond length.

The accuracy of the solution was investigated by checking whether the continuity conditions at the interface and the boundary conditions were satisfied. In the bonded portion of the interface, interface elements were not necessary. Consequently, slipping or opening could not occur. Since the displacements along the interface side of an element (or any side) depend only on the displacements of the nodes on the corresponding side of the element, the displacements must be continuous across element boundaries and therefore, across the bonded part of the interface. In the closed and debonded part of the interface the radial displacements of corresponding fiber and matrix nodes at the same position along the interface in the undeformed mesh were within $0{\cdot}001\ \mu$m of each other in the deformed mesh. The axial displacements were also checked to ensure that the fiber displaced downward more than the matrix at every point along the sliding region of the interface.

In the debonded part of the interface the radial and shear stress components at corresponding nodes in the fiber and matrix were within 0·0001 MPa of each other. In the bonded portion of the interface, the finite-element code calculated the interface stresses only at the nearest integration points and extrapolated them to the interfaces, so the continuity of the radial and shear stresses could not be checked because of the error associated with extrapolation. Figure 3 shows a graph of the interface stress components from the solution of a typical polyester/epoxy push-out problem. In Fig. 3, the magnitude of the shear stress equals the coefficient of friction ($\mu = 0{\cdot}52$ was used in this case) times the magnitude of the radial stress to within 0·001 MPa over the debonded part of the interface ($z = 2480\ \mu$m to $5360\ \mu$m), and both the radial and shear stress are zero over a small open zone at the top of the interface. In the bonded part of the interface, the stresses were calculated at a particular position along the interface by averaging the stress components extrapolated from the four adjacent gauss quadrature integration points (two on either side of the interface). ABAQUS used three integration

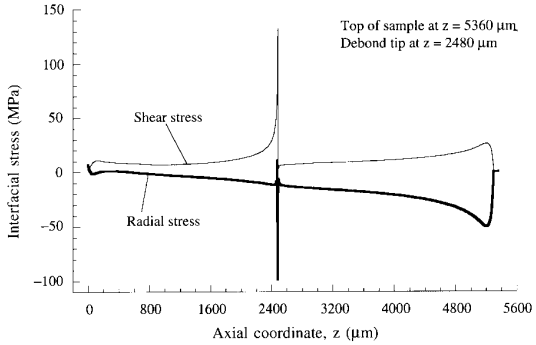

Fig. 3. Radial and shear stress along the interface for a typical polyester/epoxy problem. Fiber diameter = 1·90 mm, sample thickness = 5·36 mm, support hole diameter = 2·05 mm, and punch diameter = 1·70 mm. Constant applied displacement of $78{\cdot}65\ \mu$m plus displacement from matrix shrinkage strain of 0·0022.

points in each interface element; therefore, the stresses at each fiber and matrix node along the debonded part of interface that were reported by the finite-element code did not require extrapolation or averaging and were used directly in Fig. 3.

One difficulty with the technique is displayed in Fig. 4. Near the crack tip on the debonded side of the interface crack, Coulomb friction was satisfied, but the stresses oscillated significantly from node to node (element length in the z direction = $6{\cdot}0\ \mu$m) as the debond tip was approached. The oscillations were disregarded because, as the mesh was refined near the crack tip, the amplitude of the oscillations decreased. Although the stresses oscillated as the singularity at the crack tip was approached, the interface stresses did not oscillate as the singularity at the bottom of the interface (element length = $31{\cdot}0\ \mu$m) was approached. Kurtz and Pagano[19] reported a similar stress-oscillation phenomenon near a singularity in their elastic solution of a fiber embedded in a matrix under a thermal load. A finer mesh at the bottom of the interface captured the singularity better but did not affect the total load at the top of the fiber.

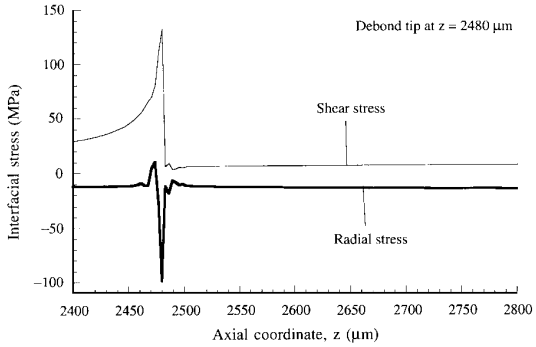

Fig. 4. Variation in interfacial stresses near the crack tip in a typical polyester/epoxy problem. Dimensions and applied displacement the same as for Fig. 3.

3 APPLICATION TO A POLYESTER/EPOXY MODEL COMPOSITE

Push-out of the top debonding system, polyester/epoxy, was modeled because experimental data were available from Bechel and Sottos[8] which not only included force, displacement and debond length but also a measurement of machine compliance and alignment. The debond length as a function of force predicted by finite-element calculations was compared to the debond length measured during progressive debonding. The push-out curve for a representative test is shown in Fig. 5. The curve labeled 'Force' is applied load (measured with a load cell) as a function of displacement which was derived from the rotation of a stepper motor. The bold plot is the corresponding measured debond length versus displacement.

Although the epoxy matrix (EPON 828/DETA) was cured at room temperature around the fully cured polyester fiber, significant chemical shrinkage of the matrix took place during cure. Evidence of the matrix shrinkage is seen in the frictional part of the curve (section III) in Fig. 5. A substantial load was needed to continue to slide the fiber within the matrix after total debond. An average radial stress at the interface was measured photoelastically and found to be $-5{\cdot}68 \pm 0{\cdot}28$ MPa. This value remained constant before and after interface debonding, indicating that the compressive radial stress distribution along the interface was solely due to processing and there was no contribution from fiber roughness. The average matrix shrinkage strain was determined to be 0·0022 with a finite-element analysis by adjusting the matrix shrinkage until the average radial stress along the interface was $-5{\cdot}68$ MPa as measured. A detailed description of the measurement of matrix shrinkage strain is contained in Bechel and Sottos,[8] Appendix A.

After processing, the ends of the sample were cut to produce parallel top and bottom faces so that the punch load could be applied perpendicular to the fiber end. The sample cutting process is difficult to simulate because the exact curvature needed before processing to result in flat faces after processing would have to be determined iteratively. Instead, the finite-element simulation began with an unloaded sample that had flat top and bottom faces and allowed the faces to be deformed as the matrix chemical shrinkage was applied.

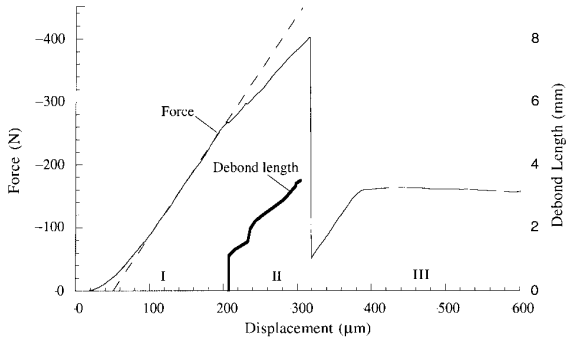

Fig. 5. Force and debond length vs displacement curves from a polyester/epoxy pushout test. Dimensions the same as for Fig. 3.

3.1 Modeling procedure

The computation of debond length is straightforward. A displacement from the progressive debonding (section II) portion of Fig. 5 was chosen and machine compliance and alignment distance were subtracted. Machine compliance is the deformation of the test fixture due to loading and was measured as $0{\cdot}42\,\mu\mathrm{m\,N^{-1}}$. The force/displacement curve shown in Fig. 5 has not been adjusted for machine compliance. Alignment distance is the displacement required to generate a load large enough for all parts of the test fixture to become seated and for the entire punch face to contact the fiber. At that displacement the machine compliance becomes a constant. The alignment distance in Fig. 5 is the point where the dashed line through the bonded part of the push-out curve crosses the displacement axis at approximately $52\,\mu$m. The chosen displacement, adjusted for machine compliance and alignment, and its corresponding force from the force/displacement curve will be referred to as d_1 and F_1, respectively.

The matrix shrinkage and this displacement, d_1, were applied to the model with an initial estimate of top debond length, and the load that developed at the top of the fiber was compared with F_1. If the force calculated was greater than the experimentally measured force, the debond length was increased to create a more compliant structure, and the finite-element analysis was conducted again for the same matrix shrinkage and applied displacement. This routine was repeated until a debond length was chosen that resulted in a load equal to F_1 at the top fiber face. These steps were conducted for several force/displacement pairs in the progressive debonding portion of the push-out data to obtain a plot of force versus debond length. The application of the displacement from the punch to the model was simplified to help make the description of the routine for debond length prediction clear. A more involved discussion of how matrix shrinkage was included in the punch displacement and the support hole boundary conditions follows.

A schematic of the boundary conditions needed to simulate the push-out test is shown in Fig. 6. Since there are several important displacements of the punch nodes (nodes at the top of the fiber where a displacement from the punch is applied) that must be discussed, Fig. 7 is provided to illustrate the relative magnitudes of these displacements. Because the interface was bonded along its entire length during processing, the chemical matrix shrinkage was first applied to the mesh with no interface debond, while the bottom node located at the edge of the hole in the sample support was fixed in the axial direction. The bottom of the sample was not forced to

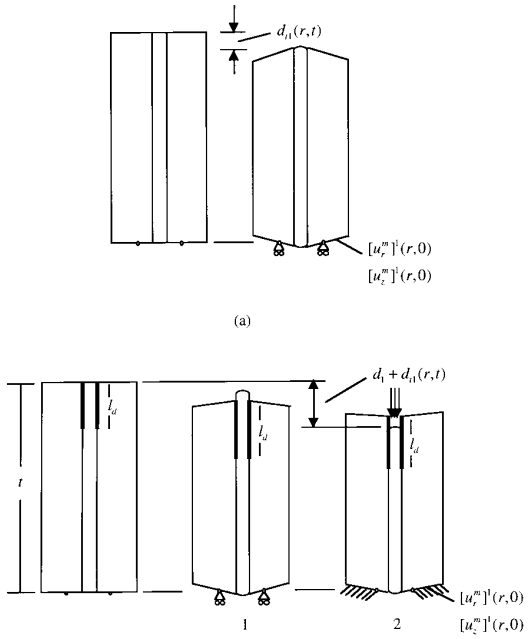

Fig. 6. Schematic of the modeling procedure for polyester/epoxy: (a) for the first finite element run, the complete interface is bonded, and (b) for the second finite-element run, a debond is added at the top of the interface.

be flat in the simulation of matrix shrinkage because the bottom of the sample was not constrained during cure. The axial displacements of the punch nodes $d_{t1}(r,t)$ and the axial and radial displacements of the bottom matrix nodes at or beyond the support hole radius, $[u_z^m]^1(r,0)$ and $[u_r^m]^1(r,0)$ were recorded. This finite-element calculation is shown schematically in Fig. 6(a).

The ABAQUS input file was then modified so the mesh was identical except that interface elements were added to simulate a debond. The matrix shrinkage was applied in step 1 of the finite-element analysis of the new mesh (see Fig. 6(b)), and in step 2 the punch nodes of the fiber were displaced to the positions where they would be after applying the matrix shrinkage to a mesh with no debond, $d_{t1}(r,t)$, plus the displacement applied by the push-out probe, d_1 (derived from the experiment). The use of $d_{t1}(r,t)+d_1$ rather than $d_{t2}(r,t)+d_1$ (Fig. 7) shows that $d_{t2}(r,t)$ in step 2 was necessary since the release of the axial stress in the fiber due to the appearance of the interface debond occurred after the fiber push-out test had commenced. When $d_{t2}(r,t)+d_1$ was used instead of $d_{t1}(r,t)+d_1$, the finite-element analysis under-predicted the slope of the fully bonded portion of the push-out data.

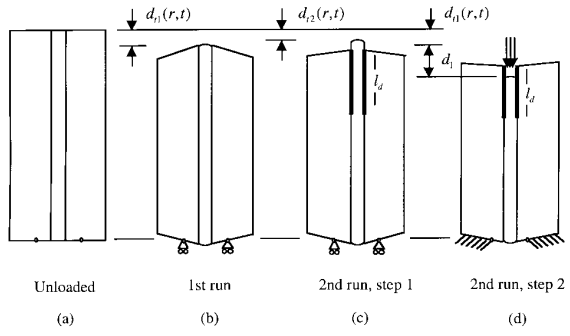

Fig. 7. Relative displacement at the top of the fiber for each phase of the polyester/epoxy finite element analysis: (a) unloaded; (b) actual deformation from matrix shrinkage; (c) matrix shrinkage with top debond; (d) displacement from pushout test added.

In step 2, the displacement of the matrix nodes at or beyond the support hold edge were constrained in the axial and radial directions to be equal to $[u_z^m]^1(r,0)$ and $[u_r^m]^1(r,0)$, respectively. This boundary condition is applied in the push-out phase to be consistent with the experiment. In both the experiment and the finite-element modeling the edges of the sample are constraint free during thermal loading, and the bottom edge of the sample contacting the support is constrained from further deformation during push-out loading.

The application of a constant displacement to the punch nodes in step 2 of the second finite-element run produced a non-uniform axial compressive stress across the top surface of the fiber which increased sharply with the radial coordinate from the center of the fiber to the punch edge. The axial stress at the punch nodes was recorded along with the radii of the punch nodes and used to calculate the total load applied to the fiber. Quadratic splines were fit through the axial stress vs r data points. The resulting continuous function, $\sigma_{zz}(r,t)$ was integrated with respect to the radial coordinate according to:

$$F = \int_0^{r_p} 2\pi r \sigma_{zz}(r,t)\, dr \tag{1}$$

to determine the total load, F, on the fiber face which was compared with F_1.

3.2 Boundary conditions

The boundary conditions and continuity conditions for the processes depicted in Fig. 6 are listed in Tables 1–3. The actual fiber push-out samples were rectangular in the r-θ plane since the front and back faces were parallel to the fiber and perpendicular to the laser beam of the polariscope used to measure debond length. The front and back faces were required to be flat and parallel to each other for the laser beam to pass through them without distortion or partial reflection.[8] The matrix radius, r_o, was taken to be half the distance between the front and back faces of the sample. The length of the debond was l_d, and the top of the sample was located at $z=t$ before the matrix chemical shrinkage was applied.

The friction between the punch face and the top of the fiber was neglected, and the friction between the bottom face of the sample and the sample support was

Table 1. Boundary and continuity conditions for matrix shrinkage of the mesh with a fully bonded interface (schematically shown in Fig. 6(a))

$z=0$	$\sigma^{f}_{rz}(r,0)=\sigma^{f}_{zz}(r,0)=0$	$0\le r\le r_f$
	$\sigma^{m}_{rz}(r,0)=\sigma^{m}_{zz}(r,0)=0$	$r_f\le r\le r_o$
	$u^{m}_{z}(r_s,0)=0$	
$z=t$	$\sigma^{f}_{rz}(r,t)=\sigma^{f}_{zz}(r,t)=0$	$0\le r\le r_f$
	$\sigma^{m}_{rz}(r,t)=\sigma^{m}_{zz}(r,t)=0$	$r_f\le r\le r_o$
$r=0$	$u^{f}_{r}(0,z)=0$	$0\le z\le t$
$r=r_f$	$\sigma^{f}_{rr}(r_f,z)=\sigma^{m}_{rr}(r_f,z)$	$0\le z\le t$
	$\sigma^{f}_{rz}(r_f,z)=\sigma^{m}_{rz}(r_f,z)$	$0\le z\le t$
	$u^{f}_{r}(r_f,z)=u^{m}_{r}(r_f,z)$	$0\le z\le t$
	$u^{f}_{z}(r_f,z)=u^{m}_{z}(r_f,z)$	$0\le z\le t$
$r=r_o$	$\sigma^{m}_{rr}(r_o,z)=\sigma^{m}_{rz}(r_o,z)$	$0\le z\le t$

approximated by fixing the bottom nodes in the r and z directions during the push-out phase of the simulation. The bottom nodes were released in the r direction for a representative case to determine the effect of representing a frictionless sample support surface. The results did not change significantly.

3.3 Debond length

The coefficient of friction was calculated with the LH and KP shear-lag solution. The equations from Kerans and Parthasarathy[5] which are discussed in the following sections are presented in Appendix A. The maximum load of -163 N and the corresponding embedded length of 5080 μm from section III of the polyester/epoxy push-out curve in Fig. 5 were used in eqn (A5) along with the matrix shrinkage of 0·0022 for the calculation of μ. The result, $\mu=0{\cdot}52$, is within the range of μ measured for several common polymers sliding against epoxy.[8]

Table 2. Boundary and continuity conditions for matrix shrinkage of the mesh with a top debond of length l_d (schematically shown in Fig. 6(b), step 1)

$z=0$	$\sigma^{f}_{rz}(r,0)=\sigma^{f}_{zz}(r,0)=0$	$0\le r\le r_f$
	$\sigma^{m}_{rz}(r,0)=\sigma^{m}_{zz}(r,0)=0$	$r_f\le r\le r_o$
	$u^{m}_{z}(r_s,0)=0$	
$z=t$	$\sigma^{f}_{rz}(r,t)=\sigma^{f}_{zz}(r,t)=0$	$0\le r\le r_f$
	$\sigma^{m}_{rz}(r,t)=\sigma^{m}_{zz}(r,t)=0$	$r_f\le r\le r_o$
$r=0$	$u^{f}_{r}(0,z)=0$	$0\le z\le t$
$r=r_f$	$\sigma^{f}_{rr}(r_f,z)=\sigma^{m}_{rr}(r_f,z)$	$0\le z\le t$
	$\sigma^{f}_{rz}(r_f,z)=\sigma^{m}_{rz}(r_f,z)$	$0\le z\le t$
	$u^{f}_{r}(r_f,z)=u^{m}_{r}(r_f,z)$	$0\le z\le t-l_d$
	$u^{f}_{z}(r_f,z)=u^{m}_{z}(r_f,z)$	$0\le z\le t-l_d$
	$\sigma^{f}_{rr}(r_f,z)=\sigma^{m}_{rr}(r_f,z)\le 0$	$t-l_d\le z\le t$
	$\lvert\sigma^{f}_{rz}(r_f,z)\rvert=\lvert\sigma^{m}_{rz}(r_f,z)\rvert\le\lvert\mu\sigma^{f}_{rr}(r_f,z)\rvert$ $=\lvert\mu\sigma^{m}_{rr}(r_f,z)\rvert$	$t-l_d\le z\le t$
	$u^{f}_{r}(r_f,z)=u^{m}_{r}(r_f,z)$ for $\sigma^{f}_{rr}(r_f,z)$ $=\sigma^{m}_{rr}(r_f,z)<0$	$t-l_d\le z\le t$
	$u^{f}_{r}(r_f,z)\le u^{m}_{r}(r_f,z)$ for $\sigma^{f}_{rr}(r_f,z)$ $=\sigma^{m}_{rr}(r_f,z)=0$	$t-l_d\le z\le t$
$r=r_o$	$\sigma^{m}_{rr}(r_o,z)=\sigma^{m}_{rz}(r_o,z)=0$	$0\le z\le t$

Table 3. Boundary and continuity conditions for fiber pushout of the mesh with a top debond of length l_d (schematically shown in Fig. 6(b), step 2)

$z=0$	$\sigma^{f}_{rz}(r,0)=\sigma^{f}_{zz}(r,0)=0$	$0\le r\le r_f$
	$\sigma^{m}_{rz}(r,0)=\sigma^{m}_{zz}(r,0)=0$	$r_f\le r\le r_s$
	$u^{m}_{r}(r,0)=[u^{m}_{r}]^{1}(r,0)$	$r_s\le r\le r_o$
	$u^{m}_{z}(r,0)=[u^{m}_{z}]^{1}(r,0)$	$r_s\le r\le r_o$
$z=t$	$u^{f}_{z}(r,t)=d_{t1}(r,t)+d_1$	$0\le r\le r_p$
	$\sigma^{f}_{rz}(r,t)=0$	$0\le r\le r_f$
	$\sigma^{f}_{zz}(r,t)=0$	$r_p\le r\le r_f$
	$\sigma^{m}_{rz}(r,t)=\sigma^{m}_{zz}(r,t)=0$	$r_f\le r\le r_o$
$r=0$	$u^{f}_{r}(0,z)=0$	$0\le z\le t$
$r=r_f$	$\sigma^{f}_{rr}(r_f,z)=\sigma^{m}_{rr}(r_f,z)$	$0\le z\le t$
	$\sigma^{f}_{rz}(r_f,z)=\sigma^{m}_{rz}(r_f,z)$	$0\le z\le t$
	$u^{f}_{r}(r_f,z)=u^{m}_{r}(r_f,z)$	$0\le z\le t-l_d$
	$u^{f}_{z}(r_f,z)=u^{m}_{z}(r_f,z)$	$0\le z\le t-l_d$
	$\sigma^{f}_{rr}(r_f,z)=\sigma^{m}_{rr}(r_f,z)\le 0$	$t-l_d\le z\le t$
	$\lvert\sigma^{f}_{rz}(r_f,z)\rvert=\lvert\sigma^{m}_{rz}(r_f,z)\rvert\le\lvert\mu\sigma^{f}_{rr}(r_f,z)\rvert$ $=\lvert\mu\sigma^{m}_{rr}(r_f,z)\rvert$	$t-l_d\le z\le t$
	$u^{f}_{r}(r_f,z)=u^{m}_{r}(r_f,z)$ for $\sigma^{f}_{rr}(r_f,z)$ $=\sigma^{m}_{rr}(r_f,z)<0$	$t-l_d\le z\le t$
	$u^{f}_{r}(r_f,z)\le u^{m}_{r}(r_f,z)$ for $\sigma^{f}_{rr}(r_f,z)$ $=\sigma^{m}_{rr}(r_f,z)=0$	$t-l_d\le z\le t$
$r=r_o$	$\sigma^{m}_{rr}(r_o,z)=\sigma^{m}_{rz}(r_o,z)=0$	$0\le z\le t$

Force vs debond length was calculated from the compliance of the polyester/epoxy push-out curve of Fig. 5 during progressive debonding. The finite-element results are shown in Fig. 8 along with the shear-lag predicted debond length for $\mu=0{\cdot}52$. Debond length was determined from shear lag by using eqns (A1) and (A2) of Appendix A first to calculate interfacial critical energy release rate (389 J m^{-2}) and then debond length as a function of applied load. The first measurable debond length was 1·1 mm at an adjusted displacement of 43·7 μm, therefore only displacements greater than 43·7 μm and the corresponding load from the push-out test of -267 N were modeled. The finite-element calculated debond length for $\mu=0{\cdot}52$ not only shows a large improvement over the shear-lag calculated debond length but also tracks the measured debond length within 7%.

4 INFLUENCE OF COEFFICIENT OF FRICTION

4.1 Shear-lag coefficient of friction

Some question remains about the accuracy of the coefficient of friction, since it was obtained with shear-lag

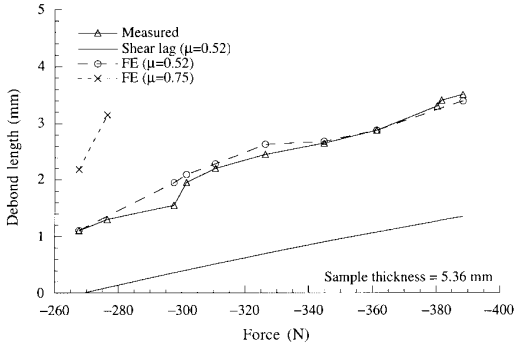

Fig. 8. Comparison of measured, shear lag and finite element calculated debond length as a function of force ($\mu = 0{\cdot}52$, $\mu = 0{\cdot}75$).

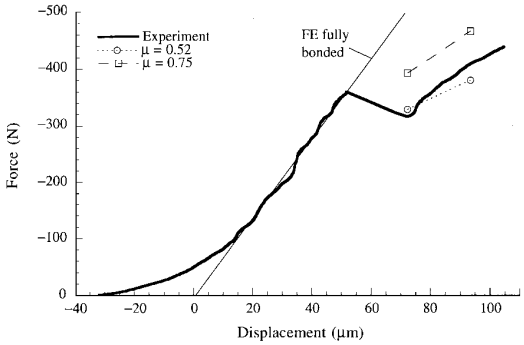

Fig. 10. Force/displacement curve from polyester/epoxy sample 2 and predicted loads for two coefficients of friction.

theory which under-predicts the debond length during progressive debonding. Figures 9–11 display results which corroborate the coefficient of friction of 0·52 without using the frictional data or shear lag. The force/displacement curves from the progressive debonding portion of three separate push-out tests (all on polyester/epoxy) are shown. These three push-out samples were chosen because their interface strengths and dimensions made them fundamentally different from each other while still being composed of the same materials. The three samples that correspond to Figs 9–11 will be referred to as samples 1, 2 and 3, respectively.

The debond length was measured during the progressive debonding phase of each of the push-out tests and used in the finite-element analysis to predict the force/displacement curve for various coefficients of friction. The measured debond length and corresponding displacement were input into the finite-element simulation and the resulting force was calculated—as opposed to force and displacement being used to determine debond length as in Section 3.3. The finite-element calculated plots of force versus displacement in Fig. 9 show that $\mu = 0{\cdot}52$ most closely reproduces the force/displacement (adjusted for machine compliance and alignment) curve of the push-out test on sample 1.

Figure 10 shows the push-out curve from sample 2 which had the same dimensions as sample 1. The only difference between samples 1 and 2 was the interface bond strength. The interface in sample 1 had a greater resistance to cracking than the interface in sample 2, as evidenced by the greater loads required in sample 1 to grow debonds of equal length. Figure 11 contains push-out data from sample 3, which was 20% longer than sample 1. Based on the measured debond length vs displacement, forces were computed using μ equal to 0·52 and 0·75 for samples 2 and 3. The computed forces shown in Figs 10 and 11 indicate that a coefficient of friction of 0·52 produced forces closer to those experimentally measured than $\mu = 0{\cdot}75$ for both a sample of different size than sample 1 and a sample of identical size but greater interface strength than sample 1.

From the parametric study of Fig. 9, the coefficient of friction was obtained independent of frictional push-out data. In other words, the measured debond length which is normally not known was used to find μ from the force/displacement data of one sample (sample 1). The fact that $\mu = 0{\cdot}52$ is consistent in polyester/epoxy for prediction of several debond lengths during a single push-out test and also for samples of varying size and with slightly varying interface resistance to cracking is significant evidence that shear-lag theory is able to

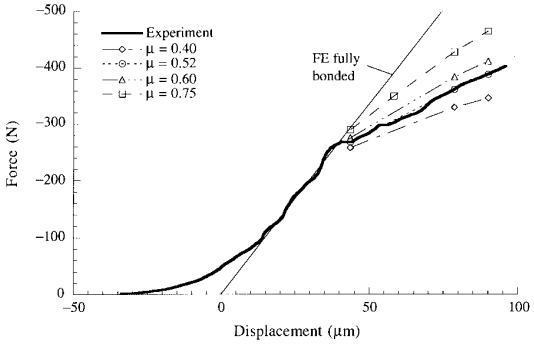

Fig. 9. Force/displacement curve from polyester/epoxy sample 1 and predicted loads for four coefficients of friction.

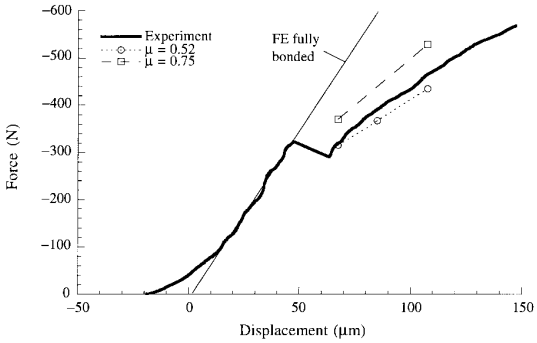

Fig. 11. Force/displacement curve from polyester/epoxy sample 3 and predicted loads for two coefficients of friction.

accurately calculate the coefficient of friction despite being inaccurate during progressive debonding.

Several differences in the conditions present before and after total debond contribute to shear lag's improved performance when modeling frictional push-out from when modeling progressive debonding. During frictional push-out, the debond length does not have to be predicted because embedded length is used. The LH and KP shear-lag formulation of equilibrium depends on an assumption of a nearly constant axial stress across each cross-section of the debonded part of the fiber. Near the interface debond tip, the stresses change rapidly, therefore the assumption of a constant axial stress on a fiber cross section will be less accurate when the debond tip is present. During frictional push-out a crack tip is not present as it is during progressive debonding. By definition, the debond length during frictional push-out is longer than during progressive debonding (greater by a factor of at least 1·5 in the current push-out tests) so the assumption of plane stress over the debonded part of the fiber used when calculating residual radial stress on the interface is approximated more closely.

The punch loads during frictional push-out are lower than during progressive debonding (by less than half in the current push-out tests) so the length of interface that is opened is presumably smaller. Shear-lag theory does not allow the interface to open so a smaller open zone will lead to a more accurate result. The axial residual force in the fiber away from the fiber ends, P_r, calculated for the shear-lag solution was based on assuming a constant residual axial strain of $\Delta\alpha\Delta T$ in the fiber. This results in P_r being constant along the fiber, but P_r is not constant through the thickness of the sample, since it must be zero at the top and bottom face of the fiber. The quantity P_r is used in the derivation of the progressive debonding shear-lag relation (eqn (A2)) but is not used in the derivation of the frictional push-out shear-lag relation between force and displacement (eqn (A5)). Any error associated with P_r does not carry over to the frictional push-out relation.[4,5]

Not only are the assumptions of shear lag approximated more closely during frictional push-out than during progressive debonding, previous results are available in the literature to support the use of shear lag for modeling frictional data. Shear lag was shown by Mackin *et al.*[20] to predict both the magnitude and the slope of fully slipping push-out data using a constant coefficient of friction when sapphire fibers were pushed from a glass matrix until the embedded length was less than half of the sample thickness.

4.2 Finite-element coefficient of friction

A more rigorous analysis of the frictional problem (loading after total debond) was attempted to try to verify the coefficient of friction calculated with shear lag, but when the finite-element method was used to determine μ, several problems were encountered. The boundary and continuity conditions of Tables 2 and 3 were applied in two steps with $l_d = t$ and with an applied displacement that caused slippage of the entire interface. To suppress the solution corresponding to rigid body motion of the fiber, a linear spring boundary condition was added at the center of the fiber along $z = 0$ with its axis parallel to the z axis. A spring stiffness of $10^{-6}\,\mathrm{N}\,\mu\mathrm{m}^{-1}$ was used. For the displacement produced at the point $r = 0$, $z = 0$ by displacing the top face of the fiber until the entire interface just began to slip, the spring developed a negligible load of less than 0·0001% of the total load at the top of the fiber.

Tandon and Pagano[17] also solved the fully slipping problem using their concentric cylinders model. The results from shear lag, finite-element analysis, and Tandon and Pagano[17] are plotted in Fig. 12. A horizontal dashed line at -163 N was also included to show where the data from each model achieved the maximum applied load measured experimentally after total debond. The finite-element analysis computed a coefficient of friction of 0·75 which is in agreement with $\mu = 0{\cdot}78$ determined by Tandon and Pagano,[17] while the shear-lag coefficient of friction was significantly lower (0.52).

When a coefficient of friction of 0·75 was used in the finite-element analysis for the displacements and corresponding loads applied during progressive debonding, the predicted debond lengths were larger than the measured debond lengths by as much as a factor of 2·5 for loads from the initial part of progressive debonding as shown in Fig. 8. For the later part of progressive debonding, debond lengths approaching the thickness of the sample still produced loads larger than the loads measured experimentally, so there is no plot of predicted debond length from the finite-element analysis ($\mu = 0{\cdot}75$) for loading beyond -276 N. Also, in Figs 9–11, the loads calculated from the measured debond lengths and their corresponding displacements using $\mu = 0{\cdot}75$ are greater than the measured loads in all three cases and significantly less accurate than when $\mu = 0{\cdot}52$ is used.

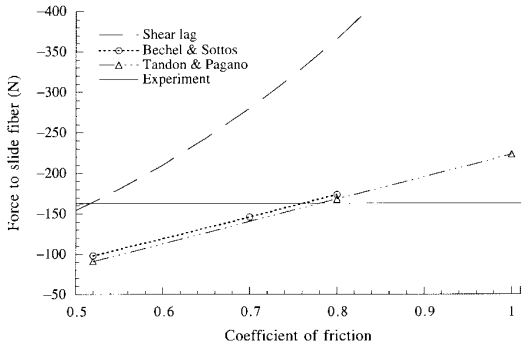

Fig. 12. Coefficient of friction vs force for fully slipping problem computed by the LH and KP shear-lag theory, finite-element analysis, and Tandon and Pagano.[17]

If the shear-lag theory is accepted as being accurate in the case of polyester/epoxy when modeling frictional push-out, then the coefficient of friction from finite-element modeling, a more rigorous formulation, should have agreed with the μ calculated with shear lag. A possible source of the difference in the μ's may be that the coefficient of friction increased as the polyester fiber slid. Increasing friction due to asperities breaking from the fiber surface and increasing the radial misfit between the fiber and matrix has been observed in previous push-out tests on SiC/Ti alloy composites.[21,22] Increasing friction is not likely in the current experiments because the measured average radial stress remained constant before and after debonding and sliding.

A more likely explanation is that the finite-element solution of the fully slipping problem is inaccurate. There were some difficulties associated with the finite-element solution of fully slipping problems that were not observed when modeling progressive debonding problems. If a constant load was applied to the top of the fiber, the fully slipping problem was unstable. As the entire fiber began to slip, a smaller load was required to slide it further. If a constant displacement was applied to the top of the fiber, the solution that minimized potential energy was a rigid body movement of the entire fiber. No axial stress developed in the fiber, and a zero punch load resulted.

To get a solution other than the rigid body solution, a relatively compliant spring was attached from ground to the bottom of the fiber. (Tandon and Pagano[17] similarly used an elastic foundation over the bottom surface of the fiber.) Varying the stiffness of the spring by plus or minus an order of magnitude did not change the results. While the solution's indifference to the stiffness of the spring is encouraging, it is not conclusive that the spring technique yields an accurate solution. When a displacement was applied to the top of the fiber which was much greater than the displacement to initiate slipping in the entire interface (displacements as great as 20% of the sample thickness), the punch load that was calculated remained constant (−163 N). The magnitude of the load should have decreased as the embedded length decreased. The polyester fibers were not pushed far enough in the current push-out tests to make it possible to measure the slope of the push-out data during frictional push-out, but intuitively the slope should be negative since a smaller portion of the fiber surface is in contact with the matrix as the fiber is pushed out. The finite-element solution of the fully slipping problem predicts a zero slope.

These points indicate that the finite-element solution of the fully slipping problem should be investigated further. The more rigorous formulation introduces additional problems. A dynamic formulation may be necessary to overcome the problems associated with the fully slipping problem. At the current time, the evidence supporting the use of shear lag for calculating μ is more compelling than the evidence supporting the use of the finite-element method with the spring boundary condition.

5 ENERGY-RELEASE RATE

Finally, the critical energy-release rate of the polyester/epoxy interface was computed using the above finite-element analysis based on the debond length, force and displacement data corresponding to the plots in Fig. 5. A coefficient of friction of $\mu = 0{\cdot}52$ (which reproduced the force/displacement curve accurately) was selected for the analysis. The finite-element simulation was run for a particular displacement and the corresponding debond length which was predicted from the compliance of the progressive debonding part of the push-out curve. The potential energy and the frictional energy dissipated during loading were recorded at the end of the finite-element simulation. The debond length was then increased by 0·1 to 0·5% (depending on the length of the debond), and an equal displacement was applied. Potential energy and the frictional energy dissipated were again recorded. The mode II critical energy-release rate was then calculated with the following equation:

$$G_{\mathrm{IIc}} = \frac{\Pi_1 - \Pi_2}{2\pi r_{\mathrm{f}}(l_{\mathrm{d2}} - l_{\mathrm{d1}})} - \frac{U_{\mathrm{f2}} - U_{\mathrm{f1}}}{2\pi r_{\mathrm{f}}(l_{\mathrm{d2}} - l_{\mathrm{d1}})} \qquad (2)$$

In eqn (2) the subscripts 1 and 2 stand for the original debond length and the incremented debond length, respectively. The symbol for potential energy is Π, and U_{f} is the frictional energy dissipated. As in earlier equations, r_{f} and l_{d} are the radius of the fiber and the debond length, respectively.

The expression for G_{IIc} given in eqn (2) is based on evaluating the rate of change of the total potential energy in the model with respect to crack growth by numerical differentiation[23] and subtracting a term that has been included to compute the rate of change of frictional energy dissipated with respect to crack growth. The calculation of the interfacial critical energy-release rate is based on the assumption that the debond length will increase by a differential increment whenever the stress state is such that the decrease in recoverable strain energy that can be gained by an increment of debond growth is equal to the energy consumed by friction during the increment of debond growth plus the energy required to debond an increment of the surface.

Several other assumptions are made when eqn (2) is used to compute G_{IIc}. The debond length is assumed to increase continuously and in a stable fashion during progressive debonding so that each load during progressive debonding is the critical load required to cause the onset of further debond growth. This assumption was not always satisfied during the push-out test. At times, the debond crack tip stopped moving briefly and later jumped forward. This problem was overcome by

calculating G_{IIc} at several debond lengths. Equation (2) is also based on the assumption that the debond tip is loaded primarily under mode II conditions. Finally, the difference between l_{d1} and l_{d2} is assumed to be small enough to approximate an infinitesimal increase in debond length. To satisfy the last assumption, the difference between l_{d1} and l_{d2} was reduced until any further reduction changed G_{IIc} by less than 1%. The finite-element mesh around the crack tip was identical for each debond length.

Another concern is the effect of including a debond in step 1 (see Fig. 6(b)) when matrix shrinkage is applied. In the experiments, debonding occurred after the push-out load was applied. Since the energy dissipation due to frictional forces is non-conservative, the frictional energy dissipation is path dependent. The finite-element analysis overestimates the frictional energy loss because it introduces an interface slip during matrix shrinkage which is opposite to the slip during push-out and which did not occur during the push-out test. This extra frictional energy dissipation could be calculated and subtracted from the total frictional energy dissipation. This subtraction was not necessary because the frictional energy dissipated in step 1 and the change in frictional energy dissipated owing to an incremental increase in debond length were three orders of magnitude less than the corresponding quantities in step 2. Therefore, this slight difference in the path to the final state had no effect on the value of G_{IIc}.

The mode-II critical energy-release rate was determined at several displacements during progressive debonding and the results are shown as a function of debond length in Fig. 13. The finite-element computed critical energy-release rate increased from about $70\,J\,m^{-2}$ to $180\,J\,m^{-2}$. The critical energy release rate ($389\,J\,m^{-2}$) obtained from the LH and KP solution by fitting the progressive debonding force/displacement data to the expression for force versus displacement during debonding from shear-lag analysis is plotted as a constant with respect to debond length. Also, shown in Fig. 13 is the critical energy-release rate ($103\,J\,m^{-2}$) obtained when the measured debond length vs force data were fit to the force vs debond length equation of the LH and KP shear-lag solution.

Several forces and the corresponding debond lengths were substituted into the shear-lag relation for force versus debond length point by point to determine whether the shear-lag calculation of critical energy-release rate also varied with debond length or remained constant. The G_{IIc} calculated point by point from shear lag decreased from $150\,J\,m^{-2}$ to $70\,J\,m^{-2}$ as the debond length increased from 1·3 to 3·3 mm. When the measured debond lengths are used in shear-lag theory instead of allowing the theory to predict debond length, the average critical energy-release rate calculated is nearly the same as the average G_{IIc} calculated with the finite-element analysis of progressive debonding data. Both averages are approximately $110\,J\,m^{-2}$. If the shear-lag theory could be modified to predict debond length more accurately, the computation of average interfacial critical energy release rate may be consistent with the average critical energy-release rate calculated with the finite-element method.

Tandon and Pagano[17] also calculated the fracture energy of the interface using eqn (2) based on the polyester/epoxy push-out data of Bechel and Sottos.[8] As Fig. 14 shows, their values for G_{IIc} also increase with debond length, have an average of approximately $110\,J\,m^{-2}$, and are within 10% of the values calculated with the finite-element solution. Both of the curves plotted in Fig. 14 are for a coefficient of friction of 0·52.

6 DISCUSSION

The finite-element method was used to derive the interface debond length as a function of force from the push-out data for a top debonding polyester/epoxy composite with relatively small residual stresses and assumed perfect bonding over the entire fiber length during processing. Debond length was computed as a function of force for samples as short as three fiber diameters to within 7% of the measured debond length when a coefficient of friction of $\mu = 0{\cdot}52$ was used. Although the

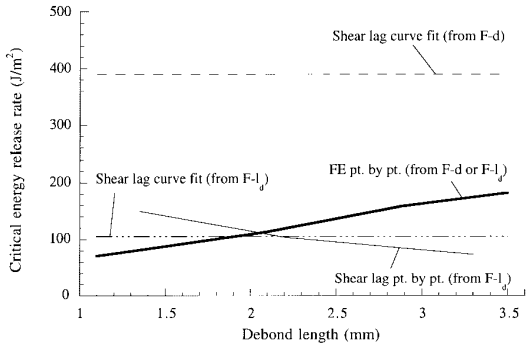

Fig. 13. Critical energy-release rate vs debond length from shear-lag theory and finite-element analysis.

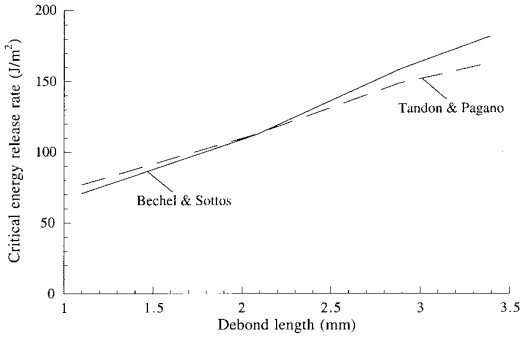

Fig. 14. Comparison of critical energy-release rate vs debond length from finite-element analysis and from Tandon and Pagano.[17]

method was more time consuming to apply than the closed form shear-lag solution, the finite-element analysis implemented for the progressive debonding portion of the push-out data was able to capture the effects of the open portions of the interface, the difference in size between the punch and fiber, and the non-uniform residual stress field. This type of analysis is required to avoid under-predicting the debond length and over-predicting G_{IIc} as the push-out samples become thin. Although the procedure described here can be used to calculate accurately debond length for a top debonding composite (even very thin samples with short debonds), the level of knowledge required about the condition of the interface and the residual stress state after processing is significant. If the assumption is made that interface debonds are not present prior to conducting a push-out test, care in sample preparation must be taken so that debonds are not introduced during curing, cutting or polishing.

The emphasis on the inability of the LH and KP shear-lag solution to calculate debond and length G_{IIc} accurately is not meant as a criticism of that model. The thicknesses of the samples that were used violated the basic assumptions of shear-lag theory, and therefore shear-lag theory did not apply to those samples. The application of the shear-lag model to the data from the thin samples was done to show the need for a more advanced method of obtaining interface properties from fiber push-out experimental data. Since this paper discusses experiments and modeling on only one material system and debonds could not be grown far from the interface, an estimate of the value of thickness vs fiber radius required for shear lag to predict debond length accurately could not be determined.

In the process of applying the shear-lag model to thin samples, it was determined that the shear-lag solution for the section III data held up under extreme conditions while the shear-lag solution for section II data broke down. This observation is important since, even if the problems with the finite-element solution of the frictional problem are rectified, the cost of running a finite-element simulation to determine μ may not be necessary. Shear-lag theory may be sufficient to compute the coefficient of friction.

The finite-element method was used to compute a coefficient of friction from the data following total debond in a representative push-out test of polyester/epoxy. The computed value of coefficient of friction agreed with the coefficient of friction from the variational model of Tandon and Pagano,[17] but was 44% greater than the coefficient of friction determined with shear-lag theory. The finite-element analysis of the fully slipping problem may be inaccurate because a boundary condition was added at the bottom of the fiber which was not applied in the experiment. The extra boundary condition, the spring at the bottom of the fiber, was required to make the problem solvable.

The results of the fracture energy computations also raise an interesting question. G_{IIc} varied by a factor of two as a function of debond length when calculated with the LH and KP shear-lag solution,[4,5] the finite-element method, and Pagano and Tandon's[17] concentric cylinders model. G_{IIc} is a property of the interface and, therefore, should be nearly uniform with respect to debond length during progressive debonding. Hutchinson and Suo[24] reviewed work on crack growth in a bimaterial interface. They noted that the apparent energy-release rate has been observed to vary with debond length. Deng[25,26] presented theoretical arguments which indicated that the change in energy-release rate as a function of debond length is due to the changing ratio of mode I to mode II loading when there is contact between the crack faces during crack growth in an interface between dissimilar materials. In the current push-out experiments (and possibly in all push-out tests) the assumption that the interface crack tip was loaded in pure shear loading may have been violated.

7 CONCLUSIONS

The finite-element method was used to predict debond length accurately during push-out testing of model polyester/epoxy samples which were thin enough that the use of shear lag was inappropriate for progressive debonding. Calculations of the interfacial coefficient of friction indicated that the LH and KP shear-lag solution was correct, based on the comparison of predicted and measured force/displacement curves in several samples with varying dimensions and interface properties.

ACKNOWLEDGEMENTS

The authors would like to acknowledge the financial support of the ONR and the AFOSR. Also, we would like to thank Dr N. J. Pagano from Wright Laboratory for his commitment to this project and Professor P. H. Guebelle from the University of Illinois for sharing his expertise on the finite-element method with us.

REFERENCES

1. Gao, Y. C., Mai, Y.-W. and Cotterell, B., Fracture of fiber reinforced materials. *J. Appl. Math. Phys.*, 1988, **39**, 550–572.
2. Marshall, D. B. and Oliver, W. C., An indentation method for measuring residual stresses in fiber-reinforced ceramics. *Mater. Sci. Eng.*, 1990, **A126**, 95–103.
3. Hsueh, C. H., Interfacial debonding and fiber pull-out stress of fiber-reinforced composites. *Mater. Sci. Eng*, 1990, **A123**, 1–11.
4. Liang, C. and Hutchinson, J. W., Mechanics of the fiber push-out test. *Mech. Mater.*, 1993, **14**, 207–221.
5. Kerans, R. J. and Parthasarathy, T. A., Theoretical analysis of the fiber pullout and push-out tests. *J. Amer. Ceram. Soc.*, 1991, **74**, 1585–1596.

6. Koss, D. A., Petrich, R. R., Kallas, M. N. and Hellmann, J. R., Interfacial shear and matrix plasticity in a metal-matrix composite. *Compos. Sci. Technol.*, 1994, **51**, 27–33.
7. Eldridge, J. I., Elevated temperature fiber push-out testing. *Mater. Res. Soc. Symp. Proc.*, 1995, **365**, 283–290.
8. Bechel, V. T. and Sottos, N. R., Application of debond length measurements to examine the mechanics of fiber push-out. *J. Mech. Phys. Solids*, 1998, **46**, 1675–1697.
9. Trimula, S., Madanaraj, H., Kaw, A. K., Besterfield, G. H. and Ye, J., Effect of extrinsic and intrinsic factors in an indentation test. *Int. J. Sol. Struct.*, 1996, **33**, 3497–3516.
10. Kallas, M. N., Koss, D. A., Hahn, H. T. and Hellmann, J. R., Interfacial stress state present in a 'thin-slice' fibre pushout test. *J. Mater. Sci.*, 1992, **27**, 3821–3826.
11. Ghosn, L. J., Kantos, P., Eldridge, J. I. and Wilson, R., Analysis of interfacial failure in SCS-6/Ti-based composites during fiber pushout testing. In *HITEMP Rev. (NASA CP-10104)*, Vol. 2, 1992, pp. 27-1–27-12.
12. Kishore, P. V., Lau, A. C. W. and Wang, A. S. D., The fiber pull-out problem: matching of singular and complete stress fields. In *Proceedings of the ASM, 6th Tech. Conf.*, 1992, pp. 1054–1063.
13. Kishore, P. V., Lau, A. C. W. and Wang, A. S. D., On fiber-matrix interfacial stresses during fiber pullout with thermal stressing. In *Proceedings of the ASM, 7th Tech. Conf.*, 1993, pp. 827–836.
14. Beckert, W. and Lauke, B., Fracture mechanics finite element analysis of debonding crack extension for a single fibre pull-out specimen. *J. Mater. Sci. Lett.*, 1995, **14**, 333–336.
15. Chandra, N. and Ananth, C. R., Analysis of interfacial behavior in MMCs and IMCs by the use of thin-slice push-out tests. *Compos. Sci. Technol.*, 1995, **54**, 87–100.
16. Tandon, G. P. and Pagano, N. J., Matrix crack impinging on a frictional interface in unidirectional brittle matrix composites. *Int. J. Sol. Struct.*, 1996, **33**, 4309–4326.
17. Tandon, G. P. and Pagano, N. J., Micromechanical analysis of unidirectional composites with frictional interfaces. Paper presented at the ASME Summer Mechanics and Materials, McNU '97, Conference, Northwestern University, Evanston, IL, 1997.
18. Hibbitt, Karlsson, and Sorenson, Inc., *ABAQUS Theory Manual*. Hibbitt, Karlsson, and Sorenson, Inc., 1994, pp. 5.1.1–5.1.3.
19. Kurtz, R. D. and Pagano, N. J., Analysis of the deformation of a symmetrically loaded fiber embedded in a matrix material. *Compos. Eng.*, 1991, **1**, 13–27.
20. Mackin, T. J., Yang, J. and Warren, P. D., Influence of fiber roughness on the sliding behavior of sapphire fibers in TiAl and glass matrices. *J. Am. Ceram. Soc.*, 1992, **75**, 3358–3362.
21. Roman, I. and Jero, P. D., Interfacial shear behavior of two titanium-based SCS-6 model composites. *Mater. Res. Soc. Symp. Proc.*, 1992, **273**, 337–342.
22. Kantos, P., Eldridge, J. I., Koss, D. A. and Ghosn, L. J., The effect of fatigue loading on the interfacial shear properties of SCS-6/Ti-based MMCs. *Mater. Res. Soc. Symp. Proc.*, 1992, **273**, 135–142.
23. Anderson, T. L., *Fracture Mechanics Fundamentals and Applications*. CRC Press, Boca Raton, FL, 1991, pp. 669–670.
24. Hutchinson, J. W. and Suo, Z., Mixed mode cracking in layered materials. *Advances Appl. Mech.*, 1992, **29**, 63–191.
25. Deng, X., An asymptotic analysis of stationary and moving cracks with frictional contact along bimaterial interfaces and in homogeneous solids. *Int. J. Sol. Struct.*, 1994, **31**, 2407–2429.
26. Deng, X., Mechanics of debonding and delamination in composites: asymptotic studies. *Compos. Eng.*, 1995, **10/11**, 1299–1315.

APPENDIX A

The following equations were derived by Kerans and Parthasarathy[5] to relate debond length and load to displacement during progressive debonding:

$$F = (C_1 G_{\mathrm{IIc}}^{1/2} + P_{\mathrm{r}} - P^*)\mathrm{e}^{C_3 \mu l_{\mathrm{d}}} + P^* \tag{A1}$$

$$d = \frac{C_2}{\mu}\left[F - C_1 G_{\mathrm{IIc}}^{1/2} - P_{\mathrm{r}} + (P^* - P_{\mathrm{r}})\ln\left(\frac{P^* - F}{P^* - C_1 G_{\mathrm{IIc}}^{1/2} - P_{\mathrm{r}}}\right)\right] \tag{A2}$$

In eqns (A1) and (A2), d is the extra punch displacement due to the growth of the interface debond (negative by convention), F is the force applied to the punch (also negative by convention), l_{d} is the debond length, and G_{IIc} is the interfacial mode II critical energy-release rate. The quantity P^* is the axial force in the fiber that would be necessary to open the debonded portion of the interface if the fiber were being pulled from the composite, and P_{r} is the thermal residual axial force in the fiber away from the fiber ends. The interface coefficient of friction is μ, and C_1,C_2 and C_3 are constants which depend on the material properties and the radius of the fiber. The axial force, P^*, is related to the thermal residual radial stress at the interface away from the fiber ends (σ_N) according to the expression

$$P^* = \frac{-\pi r^2 \sigma_N [E_{\mathrm{f}}(1 + \nu_{\mathrm{m}}) + E_{\mathrm{m}}(1 - \nu_{\mathrm{f}})]}{E_{\mathrm{m}} \nu_{\mathrm{f}}} \tag{A3}$$

where r is the fiber radius, E_{f} and E_{m} are the elastic moduli, and ν_{f} and ν_{m} are the Poisson's ratios for the fiber and matrix, respectively. The axial residual force, P_{r}, is calculated from σ_N with the following relationship

$$P_r = -P^* \nu_{\mathrm{f}}\left[\frac{P^* - 2\sigma_N \pi r^2}{P^* + 2\nu_{\mathrm{f}} \sigma_N \pi r^2}\right] \tag{A4}$$

For the frictional portion of the push-out curve (section III), a separate relationship was derived[5] to relate load and displacement

$$t + d = \frac{1}{C_3 \mu}\ln\left(\frac{P^* - F}{P^*}\right) \tag{A5}$$

The sample thickness is denoted by t. Equation (A5) was used in the current work to calculate μ from the greatest load and corresponding displacement after total debond.